Journal of Colloid and Interface Science 505 (2017) 1193–1201

Contents lists available at ScienceDirect

Journal of Colloid and Interface Science

journal homepage: www.elsevier.com/locate/jcis

Regular Article

One-pot synthesis of three-dimensional Mn_3O_4 microcubes for high-level sensitive detection of head and neck cancer drug nimorazole

Rajaji Umamaheswari [a], Muthumariappan Akilarasan [a], Shen-Ming Chen [a,c,*], Yi-Hui Cheng [a], Veerappan Mani [a,b], Sakthivel Kogularasu [a], Fahad M.A. Al-Hemaid [c], M. Ajmal Ali [c], Xiaoheng Liu [d,*]

[a] Department of Chemical Engineering and Biotechnology, National Taipei University of Technology, Taipei 106, Taiwan, ROC
[b] Graduate Institute of Biomedical and Biochemical Engineering, National Taipei University of Technology, Taipei 106, Taiwan, ROC
[c] Department of Botany and Microbiology, College of Science, King Saud University, Riyadh 11451, Saudi Arabia
[d] Key Laboratory of Education Ministry for Soft Chemistry and Functional Materials, Nanjing University of Science and Technology, Nanjing 210094, China

GRAPHICAL ABSTRACT

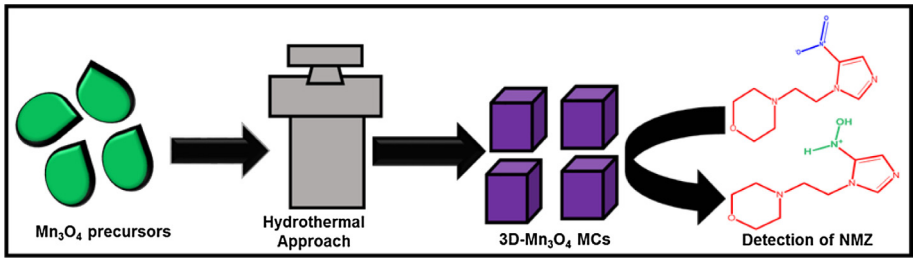

ARTICLE INFO

Article history:
Received 5 May 2017
Revised 26 June 2017
Accepted 2 July 2017
Available online 4 July 2017

Keywords:
Drug analysis
Nimorazole
Anti-cancer drug
Biosensor
Electrochemical biosensor
Modified electrode
Transition metal oxides

ABSTRACT

We described a three-dimensional Mn_3O_4 microcubes (3D–Mn_3O_4MCs) synthesised via a facile hydrothermal route for the determination of nimorazole (NMZ), an important drug that used in the treatment of head and neck cancer. The 3D–Mn_3O_4 MCs possess large active area and high conductivity, and 3D–Mn_3O_4 MCs film modified screen-printed carbon electrode (3D–Mn_3O_4MCs/SPCE) was fabricated which displayed excellent electrocatalytic ability towards NMZ. Under optimised working conditions, the modified electrode responded linearly to NMZ in the 0.025–8060 μM concentration range and the detection limit was 6 nM. A rapid, sensitive, selective, reproducible, and durable sensor was described. The practical feasibility of the sensor was demonstrated in human serum and NMZ tablet samples. The obtained results revealed the potential real-time applicability of the sensing device in biological analysis and pharmaceutical formulations.

1. Introduction

Drug analysis is an important step used to perform during various phases of pharmaceutical evaluation, including active drug monitoring through regular status and control, toxicology, stability, and other pharmacological studies [1,2]. The study mainly involves the analysis of patient samples for oral drug evolution [3] and pharmacokinetic studies [4]. In order to achieve such purposes and for measuring drugs in different media, reliable and validated analytical methods are desirable that offers direct, simple and quick determination platform requiring a minimal sample volume with purifications or pre-sampling free steps [5]. Nimorazole (4-[2-(5-nitro-1H-imidazol-1-yl)ethyl]morpholine, NMZ) is a

* Corresponding authors. Tel.: +886 2270 17147; fax: +886 2270 25238 (S.-M. Chen).
E-mail addresses: smchen78@ms15.hinet.net (S.-M. Chen), xhliu@mail.njust.edu.cn (X. Liu).

http://dx.doi.org/10.1016/j.jcis.2017.07.006
0021-9797/

synthetic nitroimidazole derivative having anti-cancer and antibacterial properties [6]. For NMZ determination, several analytical methods have been developed which includes, spectrophotometry [7], liquid chromatography [8], liquid chromatography–mass spectrometry [9–11], liquid chromatography–tandem mass spectrometry [10], high performance liquid chromatography (HPLC) [12], and electroanalytical methods [13]. However, some of these methods suffer from several problems, such as high cost, bulky and complex, long analysis time, cumbersome extraction or pre-sampling procedure, which prevent their use for routine sample analysis [14]. On the other hand, electrochemical methods are low-cost, portable, easy-to-use, fast, direct digital signal, miniaturizable and less power consumption. The electroanalytical techniques are efficient methods to study the drug reaction mechanisms at an electrode surface, which can provide insight into their metabolic fate, *in vivo* redox processes and biological activity as well [15]. However, there are no reliable electrochemical sensors based on low-cost electrode for the NMZ sensing.

Recent developments in materials chemistry research are accompanied by the synthesis of new structured metal oxide materials with novel properties [16,17]. These metal oxide materials offer excellent electronic, conductivity and catalytic properties, and electrocatalytic activity, which accelerate electron transfer between the electrode surface and redox species. These unique structured metal oxide materials have been applied to electroanalysis of drugs in various preparation methods [18–20]. The design and synthesis of unique structured metal oxide on electrode surfaces were performed to improve the sensitivity of electrochemical measurements by increasing the surface area or using the catalytic activity of metal oxide materials and the transition metal oxides have been used for the anticancer activities [21–27]. Among the transition metal oxides Mn_3O_4 materials have been also utilized as a drug in the treatment of cancer [21]. Mn_3O_4 (hausmannite) have an outstanding theoretical capacity of electrochemical activity, low-cost and have high surface area; as a result, it has been extensively employed as an electrode material in batteries and supercapacitor [28–31]. It's an important metal oxide that is widely used as an active catalyst for the oxidation of methane [32], carbon monoxide [33] and the reduction of nitro groups [34]. Although, Mn_3O_4 can be prepared by many methods, Mn_3O_4 with three-dimensional (3D) structure can be prepared by altering methods or reaction conditions. Owing to the various versatile characteristic features, including large surface area and the folded architecture of 3D network had promoted it as an attractive material for electrochemical sensor and biosensor applications.

The main objective of this work is to prepare 3D–Mn_3O_4 microcubes as a novel electrocatalyst for the electrocatalytic reduction of NMZ. Because of low-cost, easy fabrication, flexibility, and reproducibility, we adopted screen-printed carbon electrodes (SPCE) modified using 3D–Mn_3O_4 to prepare NMZ sensor. The developed amperometric sensor has displayed highly enhanced electrocatalytic activity, good sensitivity and detection limits in sub-nanomolar levels. The other advantages of the method are low over potential, enhanced signal, and quick response time.

2. Experimental

2.1. Apparatus

The electrochemical measurements were carried out using CHI 1205a workstation with a conventional three-electrode cell using SPCE as a working electrode (Area = 0.2 cm^2), Ag|AgCl (saturated KCl) as a reference electrode and Pt wire as an auxiliary electrode. Amperometric measurements were conducted using analytical rotator AFMSRX (PINE instruments, USA). EIM6ex ZAHNER (Korach, Germany) was used for performing electrochemical impedance spectroscopy (EIS) studies. Surface morphological studies were analysed using Hitachi S-3000 H Field-Emission Scanning Electron Microscope (FE-SEM). Energy-dispersive X-ray (EDX) spectra were recorded using HORIBA EMAX X-ACT (Sensor + 24 V = 16 W, resolution at 5.9 keV). Powder X-ray diffraction (XRD) studies were explored using XPERT-PRO (PAN Alytical B.V., The Netherlands) diffractometer using Cu Kα radiation. Fourier Transform Infrared spectroscopy (FT-IR) measurements were completed using Perkin Elmer spectrum RXI. Raman spectral studies were executed using Raman spectrometer (Dong Woo 500i, Korea) equipped with a charge-coupled detector.

2.2. Reagents and materials

Manganese(II) sulphate monohydrate ($MnSO_4{\cdot}H_2O$), thiourea and other chemicals were purchased from Sigma-Aldrich and used as received. SPCEs were purchased from Sensor R&D Co., Ltd., Taipei, Taiwan. All the reagents used were of analytical grade and used without any further purification. The supporting electrolyte used for the electrochemical studies was 0.1 M Phosphate buffer (PB), prepared using Na_2HPO_4 and NaH_2PO_4 and the pH was adjusted either using H_2SO_4 or NaOH. Prior to each experiment, the electrolyte solutions were deoxygenated by passing nitrogen gas for 10 min.

2.3. Synthesis of 3D–Mn_3O_4 microcubes and fabrication of modified SPCE

The 3D–Mn_3O_4 MCs were synthesised via a simple hydrothermal route as represented in Scheme 1. Briefly, 30mg of thiourea and 67.6 mg of $MnSO_4{\cdot}H_2O$ were dissolved in distilled water (40 mL) separately. After being fully dispersed by ultrasonic agitation, the solution of $MnSO_4$ was added dropwise into the solution of thiourea. The obtained mixture was stirred for 30 min to acquire a homogeneous solution. The resultant solution was transferred to a Teflon-lined stainless steel autoclave and hydrothermally treated at180 °C for 10 h. After the completion of reaction, the reddish product was collected and washed with ethanol and dried at 60 °C for overnight. The product was transferred to a tube furnace, heated to 400 °C at a heating rate of 2 °C min^{-1}, and kept at that temperature for 2 h. Finally, the product three-dimensional Mn_3O_4 microcubes (3D–Mn_3O_4 MCs) were dispersed in ethanol via ultrasonication to obtain 1 mg mL^{-1}. Next, 6 μL dispersion of 3D–Mn_3O_4 MCs were dropped at the SPCE surface and dried at room temperature.

3. Results and discussions

3.1. FESEM, EDX and mapping of 3D–Mn_3O_4 MCs

The FESEM images of 3D–Mn_3O_4 MCs were shown in Fig. 1A and B. The overall view of 3D–Mn_3O_4 MCs revealed the presence of several 3D cube-shaped particles and the side view of a microcube exposed the smooth and clean surface. The size of the microcubes was in the range of micrometre. The microcubes were well separated from each other and there were no aggregations between cubes and the 3D structure, rough surface and high crystallinity jointly furnished large surface area, which is highly beneficial in electrochemical sensing, due to the large surface area of 3D–Mn_3O_4 MCs it achieves the abundant catalytic sites on its microcubes. The EDX profile of 3D–Mn_3O_4 MCs exhibited elemental signals of Mn and O with weight percentages of 41.26, and 58.74, respectively, while their corresponding atomic percentages were of 35.20, and 64.80, respectively (Fig. 1C). The EDX mapping of

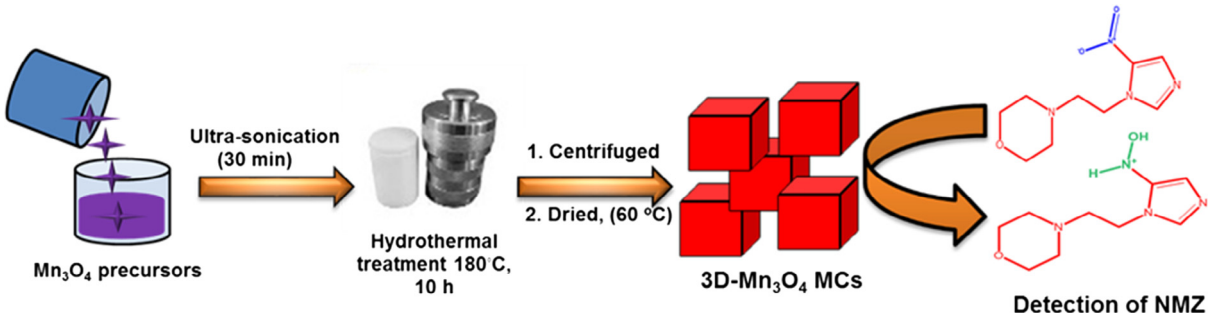

Scheme 1. Schematic representation for the synthesis of 3D–Mn_3O_4MCs and its application towards the determination of NMZ in biological and pharmaceutical samples.

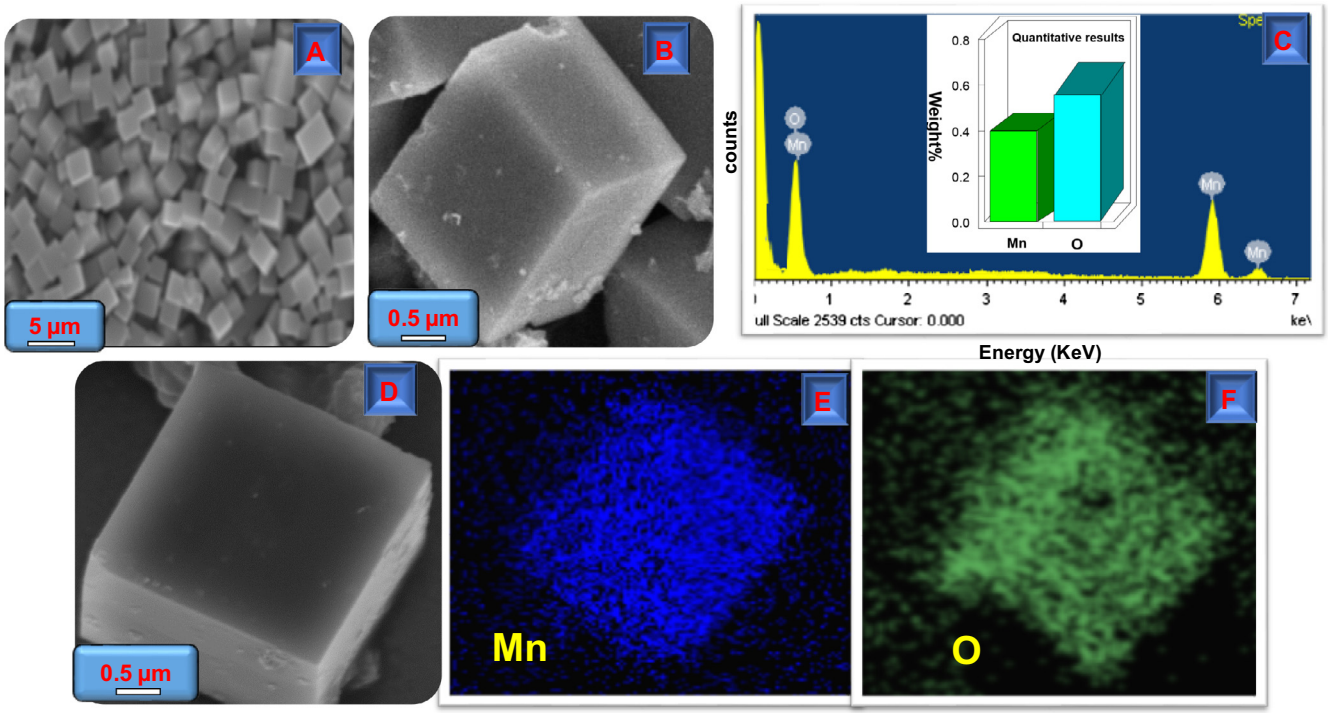

Fig. 1. FESEM images of 3D–Mn_3O_4MCs overall image (A) and side view of a microcube (B). EDX profile and quantitative result (insert) (C), and mapping of 3D–Mn_3O_4MCs (D–F).

3D–Mn_3O_4 MCs displayed the distribution profile of Mn and O elements on the surface (Fig. 1D–F).

3.2. XRD patterns, Raman, FT-IR and impedance spectral studies

Fig. 2A presented the XRD pattern of 3D–Mn_3O_4MCs which sketched peaks at 2θ of 18.7° (1 0 1), 28.4° (1 1 2), 32.3° (2 0 0), 32.7° (1 0 3), 35.6° (2 1 1), 39.4° (0 0 4), 43.7° (2 2 0), 50.9° (1 0 5), 52.6° (5 1 3), 57.1° (3 0 3), 58.3° (3 2 1), 62.2° (2 2 4), and 64.7° (4 4 0). These peaks were consistent with the standard XRD data of Mn_3O_4 MCs (JCPDS No. 24-0734) [35–39], hence confirmed the crystal structure of as-prepared microcubes [40].

Raman spectrum of the synthesised sample exhibited by Fig. 2B. Three peaks at 317 cm^{-1}, 366 cm^{-1}, and 653 cm^{-1} can be observed. The Raman spectrum of bulk Mn_3O_4 MCs ($MnMn_2O_4$ in spinel notation) was characterised by a very sharp peak at 653 cm^{-1}, this peak is responsible for the Mn-O breathing vibration of trivalent manganese ions in tedrahedral coordination. Two smaller peaks at 317 cm^{-1} and 366 cm^{-1} were also observed, similar results were found for Mn_3O_4 nanoparticles [41,42].

Fig.2C shows the FT-IR spectrum of Mn_3O_4 MCs. Mainly, two sharp peaks at 562 cm^{-1} and 761 cm^{-1} were observed, which corresponds to the Mn—O bending and stretching vibrations in the spectrum is indicative of a tetragonally distorted cubic lattice. These peaks may be due to the coupling mode between Mn—O stretching modes of tetrahedral and octahedral sites, which confirms the presence of Mn_3O_4 MCs. Similar reports were found for Mn_3O_4 MCs [43].

EIS analysis has been carried out to study the electrical and interfacial properties of the fabricated films modified electrodes [44]. Fig. 2D displays the EIS curves obtained at SPCE (a), 3D–Mn_3O_4MCs/SPCE (b) in 0.1 M KCl containing 5 mM $Fe(CN)6^{3-/4-}$. Randles equivalent circuit model was adopted to fit the experimental data wherein, R_s, R_{ct}, C_{dl} and Zw are stands for electrolyte resistance, charge transfer resistance, double layer capacitance and Warburg impedance (inset to Fig. 2D). The results were exemplified as Nyquist plots. The observed semicircles portions of the EIS curves indicates the parallel combination of R_{ct} and C_{dl} at electrode surface resulting from electrode impedance and the linear portions of the curves represents diffusion limited process. The charge transfer resistance (R_{ct}) values obtained at unmodified SPCE,

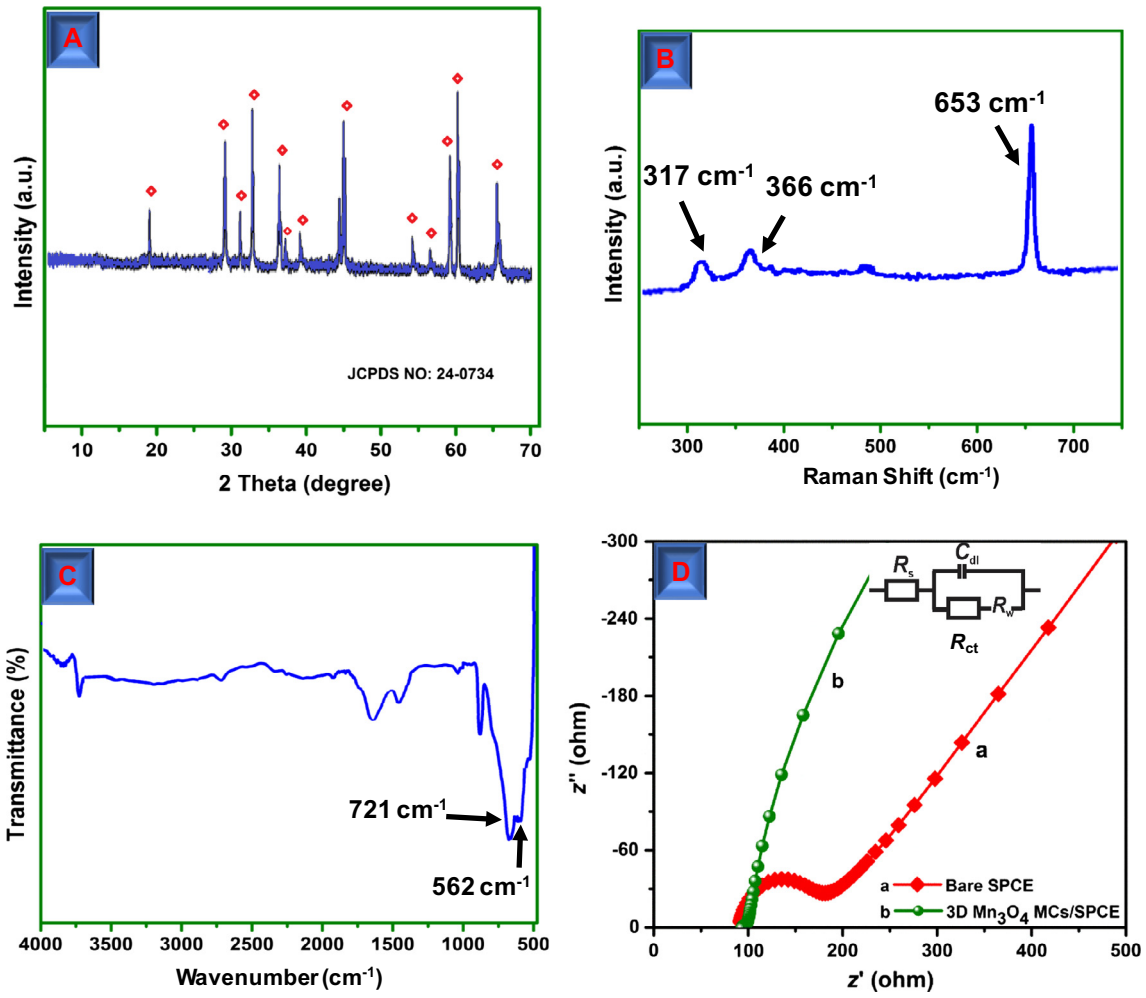

Fig. 2. (A) XRD, (B) Raman and (C) FTIR spectra of 3D–Mn_3O_4MCs, and (D) EIScurves of unmodified SPCE (a), 3D–Mn_3O_4MCs/SPCE (b) in 0.1 M KCl containing 5 mM $Fe(CN)_6^{3-/4-}$. Amplitude = 5 mV, Frequency: 0.1 Hz to 100 kHz. Inset: Randles equivalent circuit used to fit the data; R_s, R_{ct}, C_{dl}, and Z_w are electrolyte resistance, charge transfer resistance, double layer capacitance and Warburg impedance, respectively.

3D–Mn_3O_4MCs/SPCE were 91.45 Ω and 4.23 Ω, respectively. The R_{ct} values are in the following order; unmodified SPCE > 3D–Mn_3O_4MCs/SPCE, respectively. Obviously, the EIS results revealed that the 3D–Mn_3O_4MCs/SPCE material interface has high electrical conductivity.

3.3. Electrocatalytic activity of 3D–Mn_3O_4 MCs/SPCE towards NMZ reduction

Next, the electrochemical activity of 3D–Mn_3O_4 MCs was investigated. Fig. 3A illustrated the cyclic voltammograms (CVs) of SPCE (a), and 3D–Mn_3O_4 MCs (b) over a potential range of −0.38 V to 0.48 V (vs. Ag/AgCl) at a scan rate of 2 mV s^{-1}. The CV of 3D–Mn_3O_4 MCs exhibited enhanced background current in comparison with control electrode. Two redox couples, −0.24 V/−0.28 V (I/II) and −0.04 V/−0.15 V (III/IV) corresponding to reversible reactions of Mn_3O_4/MnOOH and MnOOH/MnO_2 were observed and those are characteristic voltammetric behaviour of electrochemically active 3D–Mn_3O_4 MCs [45].

Electrocatalytic ability of the 3D–Mn_3O_4/SPCE towards electrocatalysis of NMZ (50 μM) reduction is investigated in phosphate buffer (pH 7.0) (Fig. 3B). The forward segment of first cycle displayed a sharp cathodic peak at −0.60 V, which is manifested to the reduction of NO_2–NMZ to NHOH–NMZ (Eq. (1)). An oxidation peak is observed at +0.1 V in the backward segment, which is related to the oxidation of NHOH–NMZ to NO–NMZ and this reaction is reversible and hence corresponding reduction is also observed at −0.32 V during the second cyclic run. This type of electrocatalytic behaviour is consistent with the previous reports [14,46–50].

$$\mathbf{NO_2{-}NMZ} + \mathbf{4e^-} + \mathbf{4H^+} \rightarrow \mathbf{NHOH{-}NMZ} - \mathbf{2e^-} - \mathbf{2H^+} \leftrightarrows \mathbf{NO{-}NMZ} + \mathbf{2e^-} + \mathbf{2H^+} \quad (1)$$

In this study, we focused on the reduction peak of NMZ (NO_2–NMZ to NHOH–NMZ). Accordingly, the NMZ reduction at 3D–Mn_3O_4/SPCE was monitored and compared with control electrodes. In comparison with control electrodes (bare SPCE, and 3D–Mn_3O_4/SPCE), the 3D–Mn_3O_4/SPCE is shown significantly enhanced reduction peak current. The observed over potentials at bare SPCE, and 3D–Mn_3O_4 MCs/SPEC are −0.78 V, and −0.6 V, respectively. The over potential at 3D–Mn_3O_4/SPCE is 180 mV lower than the bare SPCE. The drastic shift in the over potential at 3D–Mn_3O_4/SPCE is due to the electrocatalytic activity of 3D–Mn_3O_4, which greatly accelerates and catalyzes the reduction process. Thus, the 3D–Mn_3O_4 MCs/SPEC exhibited excellent electrocatalytic ability towards the reduction of NMZ, which is obvious from the observed high faradaic current and minimised over potential. This can be attributed to the large surface area, high conductivity, the3D structure of Mn_3O_4 and abundant catalytic sites on the cubes.

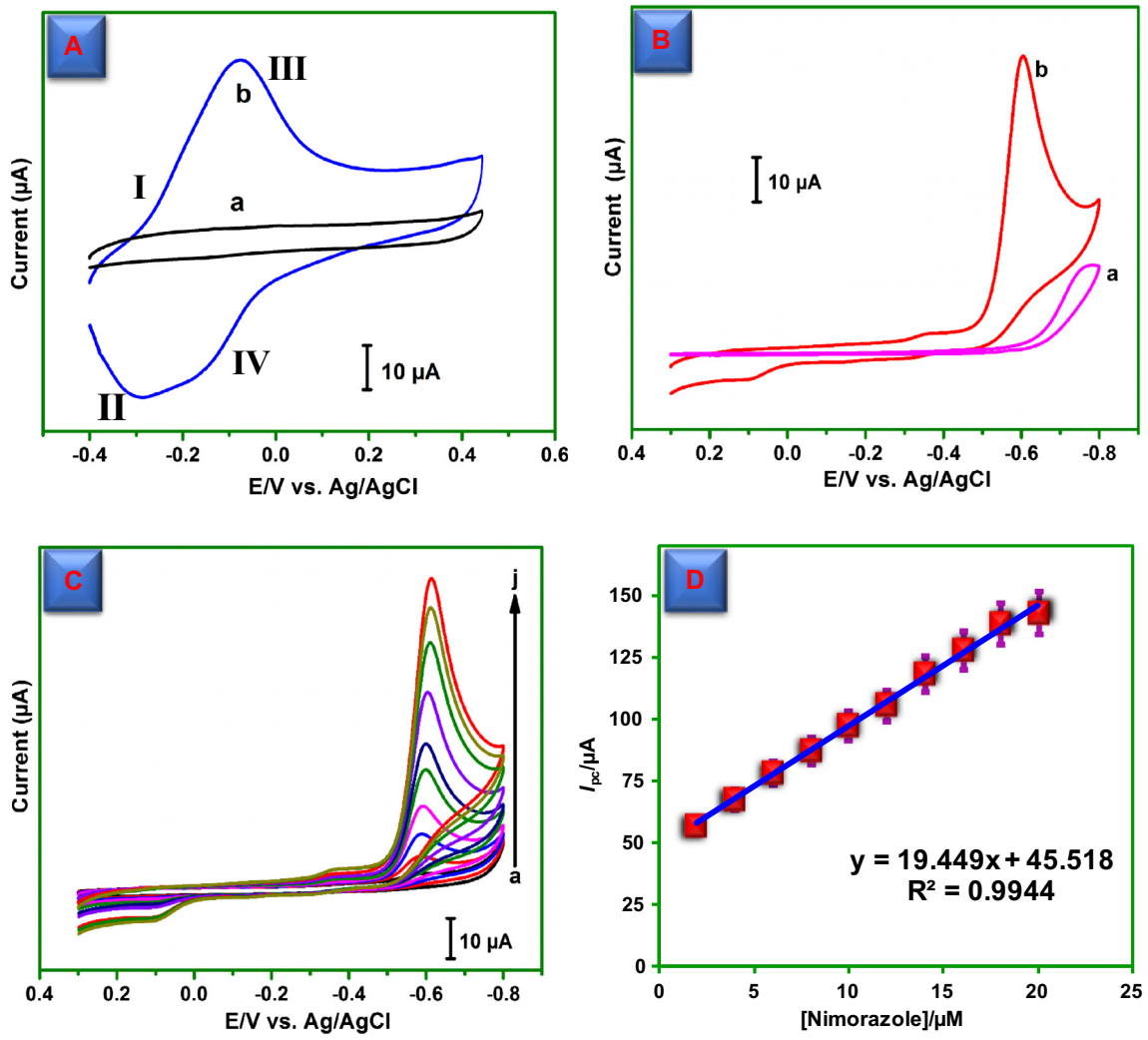

Fig. 3. (A) CVs obtained at Bare SPCE (a), and 3D–Mn_3O_4 (b), films modified SPCEs in 0.1 M NaOH at scan rate of 2 mV s^{-1}. (B) Cyclic voltammograms obtained at bare SPCE (a), and3D–Mn_3O_4MCs/SPCE(b) in PB (pH 7.0) containing 50 μM NMZ at the scan rate of 50 mV s^{-1}. (C) Cyclic voltammogram obtained at 3D–Mn_3O_4/SPCE in PB (pH 7) in different concentrations of NMZ (a = 50, b = 100, c = 150, d = 200, e = 250, f = 300, g = 350, h = 400, i = 450, and *j* = 500 μM). (D) Calibration plot, cathodic peak current (I_{pc})/μA vs. [NMZ]/μM.

Fig. 3C displayed the CVs obtained at 3D–Mn_3O_4 MCs/SPCE towards different concentrations of NMZ in PB (pH 7). As can be seen from the figure, the peak current was increased linearly as the concentration of NMZ increased over a linear range of 50–500 μM with a correlation coefficient of 0.994 (Fig. 3D). Thus, the modified electrode is capable of providing linear responses towards NMZ and the obtained good linearity is indicating anti-fouling nature of the electrode surface.

3.4. Effect of scan rate and pH dependence

Next, the effect of scan rate on the reduction of NMZ was studied by applying different scan rates (Fig. 4A). The cathodic peak current was linearly increased as the scan rate increased over the studied range from 0.02 to 0.2 V s^{-1}. The plot between reduction peak current and the square root of scan rate exhibited linear relationship, which revealed the diffusion controlled electrocatalytic process of NMZ at the modified electrode (Fig. 4B). The influence of buffer pH on the electrochemical response of 3D–Mn_3O_4/SPCE towards 50 μM NMZ was investigated (Fig. 4C). As the pH of supporting electrolyte varied, the peak current and potential corresponding to NMZ reduction were changed. The NMZ reduction peak current increased as the pH increases from 3.0 to 7.0 and reached maxima at pH 7. From pH 7.0 to pH 11.0, the peak current gradually decreased. Thus, the reduction of NMZ at modified electrode was more favourable at pH 7.0; therefore, we set this pH as optimum pH for established NMZ sensor. The plot between different pH and peak potential was also exhibited a linear behaviour (Fig. 4D).

3.5. 5Amperometric determination of NMZ

Fig. 5A displayed the amperometric responses of 3D–Mn_3O_4-MCs film modified rotating electrode upon following successive injections of aliquots of NMZ into PB (pH 7.0) at regular intervals of the 50 s. The rotation speed of the electrode was set at 1200 RPM and the electrode potential (E_{app}) was applied as −0.54 V. Clearly defined and steady amperometric responses were observed for each addition of NMZ. The steady state current was reached in less than 5 s revealing quick sensor response. The response current was increased linearly as the concentrations of NMZ. The working range of the sensor was 0.025–8060 μM and the corresponding regression equation was, $I_{pc}/\mu A = 0.4958$ [NMZ]/μA μM^{-1}; with the correlation coefficient of 0.9945

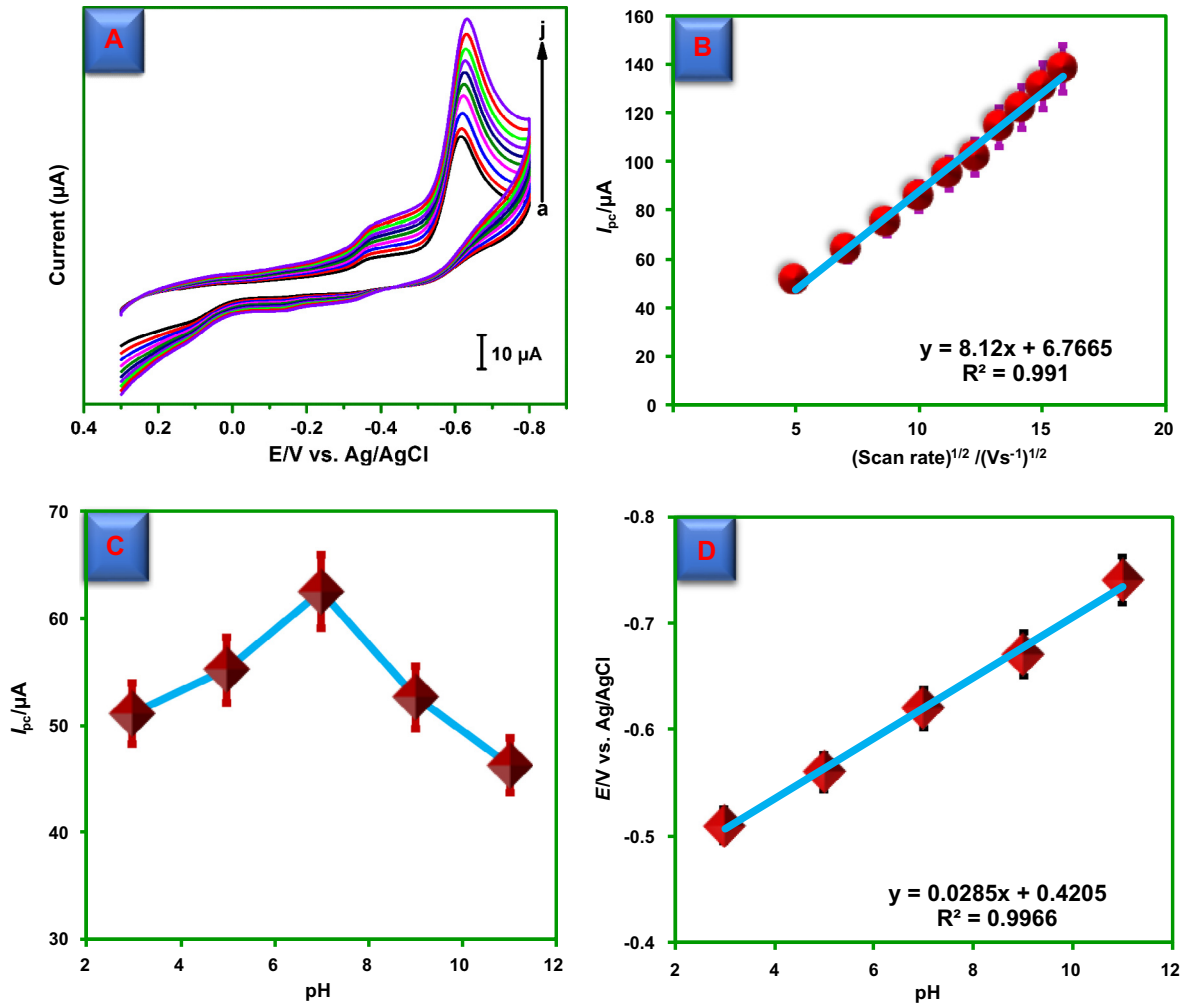

Fig. 4. (A) Cyclic voltammograms obtained at 3D–Mn_3O_4MCs/SPCE in PB (pH 7.0) containing 50 μM NMZ at different scan rates (a = 0.02, b = 0.04, c = 0.06, d = 0.08, e = 0.10, f = 0.12, g = 0.14, h = 0.16, i = 0.18 and *j* = 0.20 V s^{-1}. (B) (Scan rate)$^{1/2}$/(V s^{-1})$^{1/2}$ vs. peak currents (μA), (C) Plot of peak current (μA) vs. pH, and (D) Plot between peak potential (V) vs. pH For pH studies, the cyclic voltammograms were carried out in supporting electrolyte of different pH containing 50 μM NMZ at a scan rate of 0.50 V s^{-1}.

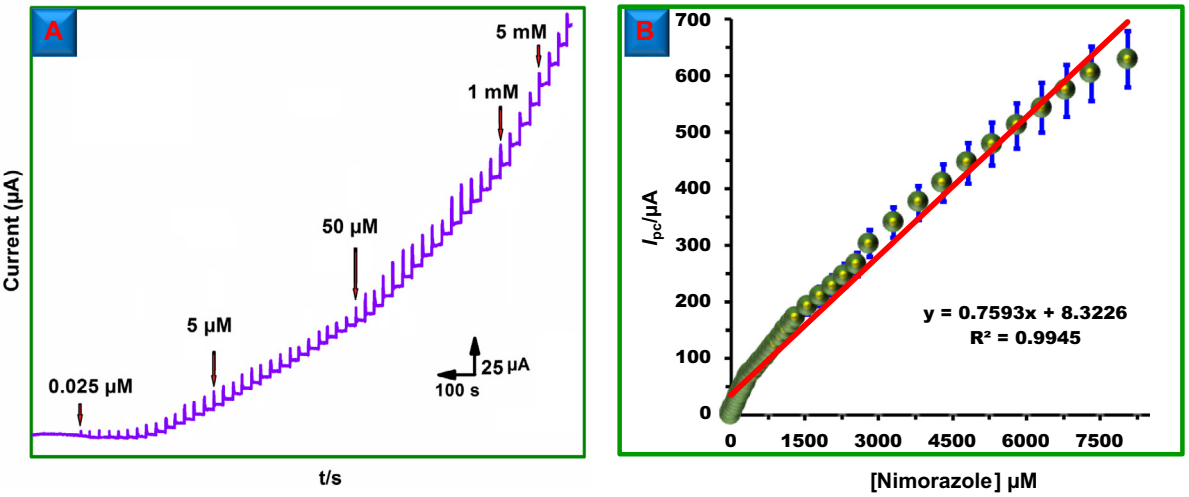

Fig. 5. (A) Amperometric response of 3D–Mn_3O_4MCsfilm modified rotating disk electrode towards each sequential additions of NMZ into PB (pH 7.0). The rotation speed of the electrode was 1200 RPM and the electrode potential was – 0.54 V (vs. Ag/AgCl). (B) The plot between [NMZ]/μM vs. current (μA).

Table 1
Comparison of analytical parameters for the determination of NMZ at 3D-Mn_3O_4 MCs film modified SPCE with previously reported works.

Methods	Linear range	LOD	Ref.
Differential pulse polarography	0.005–10 μM	2 μM	[14]
Liquid chromatography–mass spectrometry	0.25–200 ng/mL	0.25 ng/mL	[51]
Reversed-phase high-performance liquid chromatography	20–60 μg/mL	20.62 ng/mL	[52]
Amperometry	0.025–8060 μM	6 nM	This work

(Fig. 5B). The limit of detection (LOD, S/N = 3) of the sensor was calculated to be 6 nM, while the limit of quantification (LOQ, S/N = 10) was estimated to be 20 nM. Such a low detection limit in nanomolar level and wide linear range were clearly revealing the excellent sensing attributes of the 3D–Mn_3O_4MCs film towards the determination of NMZ. The sensitivity of the sensor was 3.80 μA μM^{-1} cm^{-2}. The electroanalytical parameters achieved at 3D-Mn_3O_4 MCs were compared with previous reports as a Table 1.

3.6. Selectivity, reproducibility, repeatability, and stability

The selectivity of the modified electrode was assessed by performing amperometric analysis in presence of likely interfering compounds. Fig. 6A presented the amperometric responses of 3D–Mn_3O_4MCs/SPCE towards 5 μM NMZ (a) and 0.5 mM of NADH (b), dopamine (c), folic acid (d), uric acid (e), cysteine (f), ascorbic acid (g), guanine (h), epinephrine (i), pyridoxine (j), acetaminophen (k), benperidol (l), and 5-Fluorouracil (m). The electrode quickly responded to NMZ, but it was insensitive to all the other tested species; thus, the electrode capable of recognising NMZ specifically in presence of many similar species and this situation usually exists in biological sample analysis.

The storage stability of the described 3D–Mn_3O_4MCs/SPCE incorporated sensor has been evaluated. The electrode retained its 95.2% initial current response after 3 weeks of its storage, which validated good storage stability of the modified electrode. The good stability of the electrode could be correlated to the strong interaction of 3D-Mn_3O_4 MCs film to the electrode surface. For the reproducibility and repeatability study, sensor response of the electrode towards 50 μM NMZ was monitored. The sensor displayed good reproducibility with a relative standard deviation (R.S.D) of 3.68% for five individual measurements performed on a single modified electrode. The R.S.D for five repetitive measurements using five modified electrodes was 4.58% indicating good repeatability.

Table 2
Determination of NMZ in drug and human blood serum samples.

Real Samples	Added (μM)	Found (μM)	Recovery (%)	RSD[a] (%)
NMZ drug	1.0	0.96	96.0	3.75
	2.0	1.94	97.0	4.50
Human blood serum	1.0	0.97	97.0	3.53
	2.0	1.95	97.5	3.82

[a] Related standard deviation (RSD) of 3 independent experiments.

3.7. Real sample analysis

All the excellent sensor features of 3D–Mn_3O_4MCs/SPCE were indicating that this electrode could be suitable for real-time drug analysis in pharmaceutical and biological samples. We have performed real sample study in drug and human serum samples. The drug sample was purchased from local pharmacy, grinded and dissolved in ethanol to prepare stock solution. Human serum sample was spiked with appropriate amount of NMZ. Then, amperometric experiments were performed to detect NMZ present in the aforementioned samples using 3D–Mn_3O_4 MCs/SPCE as electrode. Aliquots of known concentrations of lab sample, NMZ tablet sample and human serum sample were injected and their corresponding amperometric responses were monitored. The signal sensitivity and response time of real samples were consistent with that of lab sample. The recoveries were calculated and found to be in the acceptable range of 96–97.5% (Table 2) and hence we believe the method can be used as reliable NMZ sensor towards real-time drug analysis.

4. Conclusions

We described the synthesis of novel 3D-Mn_3O_4MCs and characterised it through SEM, EDX, mapping, XRD, Raman, FTIR and electrochemical studies. The characterization results revealed the successful formation of high crystalline microcubes. The electrocatalytic studies revealed the superior electrocatalytic activity of 3D-Mn_3O_4 MCs/SPCE towards NMZ reduction. The effect of concentration, kinetics, and pH were optimised in order to obtain maximum sensor performance. The fabricated NMZ amperometric sensor displayed nanomolar level detection of NMZ with LOD of 6 nM and linear range of 0.025–8060 μM. Moreover, the fabricated

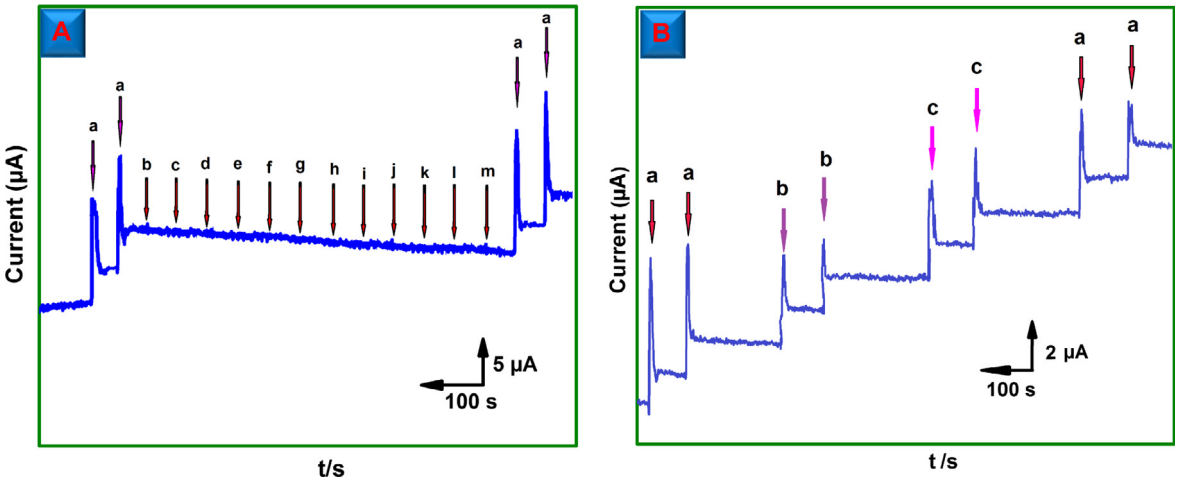

Fig. 6. (A) Amperometric response of 3D–Mn_3O_4MCs/SPCE towards 50 μM NMZ (a) and 0.5 mM of NADH (b), dopamine (c), folic acid (d), uric acid (e), cysteine (f), ascorbic acid (g), guanine (h), epinephrine (i), pyridoxine (j), acetaminophen (k), benperidol (l) and 5-Fluorouracil (m). (B) Real sample analysis: Amperometric responses of 3D–Mn_3O_4MCs/SPCE towards 1 μM NMZ, lab sample (a), NMZ tablets (b), and spiked human blood serum (c).

sensor acquired good selectivity, repeatability, reproducibility and durability. In addition, the sensor was successfully analysed the NMZ amount present in NMZ drug and NMZ spiked human serum sample. The application of this material with simple preparation steps and exceptional properties such as 3D structure, large surface area, high conductivity, long-term stability on this metal oxide. In future, 3D-Mn_3O_4 MCs can be paired with immobilized antibodies for the biosensoric detection of food allergens.

Acknowledgement

The authors extend their appreciation to the International Scientific Partnership Program ISPP at King Saud University for funding this research work through ISPP#6. This project was supported by the national science council and ministry of science and technology, Taiwan (ROC).

References

[1] A.C. Valderrama-Negrón, W.A. Alves, Á.S. Cruz, S.O. Rogero, D. de Oliveira Silva, Synthesis, spectroscopic characterization and radiosensitizing properties of acetato-bridged copper(II) complexes with 5-nitroimidazole drugs, Inorg. Chim. Acta 367 (1) (2011) 85–92.
[2] A. Rahi, N. Sattarahmady, R.D. Vais, H. Heli, Sonoelectrodeposition of gold nanorods at a gold surface–application for electrocatalytic reduction and determination of nitrofurazone, Sens. Actuat. B: Chem. 210 (2015) 96–102.
[3] J.R. Proudfoot, The evolution of synthetic oral drug properties, Bioorg. Med. Chem. Lett. 15 (4) (2005) 1087–1090.
[4] R.D. Vais, N. Sattarahmady, K. Karimian, H. Heli, Green electrodeposition of gold hierarchical dendrites of pyramidal nanoparticles and determination of azathioprine, Sens. Actuat. B: Chem. 215 (2015) 113–118.
[5] S.A. Özkan, B. Uslu, H.Y. Aboul-Enein, Analysis of pharmaceuticals and biological fluids using modern electroanalytical techniques, Crit. Rev. Anal. Chem. 33 (3) (2003) 155–181.
[6] J. Overgaard, B.S. Sorensen, J. Alsner, C. Wiuf, M. Nordsmark, K. Toustrup, Method for Determining Clinically Relevant Hypoxia in Cancer, Google Patents, 2012.
[7] P. Nagaraja, K. Sunitha, R. Vasantha, H. Yathirajan, Spectrophotometric determination of metronidazole and tinidazole in pharmaceutical preparations, J. Pharmaceut. Biomed. Anal. 28 (3) (2002) 527–535.
[8] D.D. Liana, B. Raguse, J.J. Gooding, E. Chow, Recent advances in paper-based sensors, Sensors 12 (9) (2012) 11505–11526.
[9] B. Unnikrishnan, V. Mani, S.-M. Chen, Highly sensitive amperometric sensor for carbamazepine determination based on electrochemically reduced graphene oxide–single-walled carbon nanotube composite film, Sens. Actuat. B: Chem. 173 (2012) 274–280.
[10] K. Mitrowska, A. Posyniak, J. Zmudzki, Selective determination of fourteen nitroimidazoles in honey by high-performance liquid chromatography–tandem mass spectrometry, Anal. Lett. 47 (10) (2014) 1634–1649.
[11] P. Meering, R. Baumann, J. Zijp, R. Maes, Determination of misonidazole and desmethylmisonidazole in plasma by high-performance liquid chromatography with reductive electrochemical detection, J. Chromatogr. B Biomed. Sci. Appl. 310 (1984) 159–166.
[12] P. Workman, Analysis of the basic 5-nitroimidazole nimorazole in blood by reversed-phase high-performance liquid chromatography, and its application to pharmacokinetic studies in individual mice, J. Chromatogr. B Biomed. Sci. Appl. 163 (4) (1979) 396–402.
[13] M.A. La-Scalea, S.H. Serrano, I.G. Gutz, Voltammetric behaviour of metronidazole at mercury electrodes, J. Braz. Chem. Soc. 10 (2) (1999) 127–135.
[14] P. Sivasankar, S.J. Reddy, Voltammetric behavior and measurement of nimorazole, Electroanalysis 2 (2) (1990) 171–174.
[15] S. Rauf, J. Gooding, K. Akhtar, M. Ghauri, M. Rahman, M. Anwar, A. Khalid, Electrochemical approach of anticancer drugs–DNA interaction, J. Pharmaceut. Biomed. Anal. 37 (2) (2005) 205–217.
[16] V. Mani, M. Govindasamy, S.-M. Chen, B. Subramani, A. Sathiyan, J.P. Merlin, Determination of folic acid using graphene/molybdenum disulfide nanosheets/gold nanoparticles ternary composite, Int. J. Electrochem. Sci. 12 (2017) 258–267.
[17] V. Mani, M. Govindasamy, S.-M. Chen, R. Karthik, S.-T. Huang, Determination of dopamine using a glassy carbon electrode modified with a graphene and carbon nanotube hybrid decorated with molybdenum disulfide flowers, Microchim. Acta 183 (7) (2016) 2267–2275.
[18] M. Govindasamy, S.-M. Chen, V. Mani, A. Sathiyan, J.P. Merlin, F.M. Al-Hemaid, M.A. Ali, Simultaneous determination of dopamine and uric acid in the presence of high ascorbic acid concentration using cetyltrimethylammonium bromide–polyaniline/activated charcoal composite, RSC Adv. 6 (102) (2016) 100605–100613.
[19] J. Rizzo, C. Riley, D. von Hoff, J. Kuhn, J. Phillips, T. Brown, Analysis of anticancer drugs in biological fluids: determination of taxol with application to clinical pharmacokinetics, J. Pharmaceut. Biomed. Anal. 8 (2) (1990) 159–164.
[20] R. Sasikumar, M. Govindasamy, S.-M. Chen, Y. Chieh-Liu, P. Ranganathan, S.-P. Rwei, Electrochemical determination of morin in kiwi and strawberry fruit samples using vanadium pentoxide nano-flakes, J. Colloid Interface Sci. (2017).
[21] S. Khan, A.A. Ansari, A.A. Khan, M. Abdulla, O. Al-Obeed, R. Ahmad, In vitro evaluation of anticancer and biological activities of synthesized manganese oxide nanoparticles, MedChemComm 7 (8) (2016) 1647–1653.
[22] G. Prabha, V. Raj, Sodium alginate–polyvinyl alcohol–bovin serum albumin coated Fe_3O_4 nanoparticles as anticancer drug delivery vehicle: doxorubicin loading and in vitro release study and cytotoxicity to HepG2 and L02 cells, Mater. Sci. Eng., C 79 (2017) 410–422.
[23] B.B. Manshian, S. Pokhrel, U. Himmelreich, K. Tämm, L. Sikk, A. Fernández, R. Rallo, T. Tamm, L. Mädler, S.J. Soenen, In silico design of optimal dissolution kinetics of Fe-doped ZnO nanoparticles results in cancer-specific toxicity in a preclinical rodent model, Adv. Healthc. Mater. 6 (9) (2017).
[24] A.S. Estrada-Montaño, A.D. Ryabov, A. Gries, C. Gaiddon, R. Le Lagadec, Iron (III) pincer complexes as a strategy for anticancer studies, Eur. J. Inorg. Chem. 2017 (12) (2017) 1673–1678.
[25] Y.C. Lee, I.J. Kang, Optimal fabrication conditions of chitosan−Fe_3O_4–gold nanoshells as an anticancer drug delivery carriers, Bull. Korean Chem. Soc. 38 (3) (2017) 313–319.
[26] A. Adhikari, N. Kumari, M. Adhikari, N. Kumar, A.K. Tiwari, A. Shukla, A.K. Mishra, A. Datta, Zinc complex of tryptophan appended 1, 4, 7, 10-tetraazacyclododecane as potential anticancer agent: Synthesis and evaluation, Bioorg. Med. Chem. 25 (13) (2017) 3483–3490.
[27] N. Revathi, M. Sankarganesh, J. Rajesh, J.D. Raja, Biologically active Cu (II), Co (II), Ni (II) and Zn (II) complexes of pyrimidine derivative schiff base: DNA binding, antioxidant, antibacterial and in vitro anticancer studies, J. Fluoresc. (2017) 1–14.
[28] J.W. Lee, A.S. Hall, J.-D. Kim, T.E. Mallouk, A facile and template-free hydrothermal synthesis of Mn_3O_4 nanorods on graphene sheets for supercapacitor electrodes with long cycle stability, Chem. Mater. 24 (6) (2012) 1158–1164.
[29] H. Gao, F. Xiao, C.B. Ching, H. Duan, Flexible all-solid-state asymmetric supercapacitors based on free-standing carbon nanotube/graphene and Mn_3O_4 nanoparticle/graphene paper electrodes, ACS Appl. Mater. Interf. 4 (12) (2012) 7020–7026.
[30] K.V. Sankar, D. Kalpana, R.K. Selvan, Electrochemical properties of microwave-assisted reflux-synthesized Mn_3O_4 nanoparticles in different electrolytes for supercapacitor applications, J. Appl. Electrochem. 42 (7) (2012) 463–470.
[31] X.-J. Li, Z.-W. Song, Y. Zhao, Y. Wang, X.-C. Zhao, M. Liang, W.-G. Chu, P. Jiang, Y. Liu, Vertically porous nickel thin film supported Mn_3O_4 for enhanced energy storage performance, J. Colloid Interface Sci. 483 (2016) 17–25.
[32] G.B. Hoflund, Z. Li, W.S. Epling, T. Göbel, P. Schneider, H. Hahn, Catalytic methane oxidation over Pd supported on nanocrystalline and polycrystalline TiO_2 Mn_3O_4, CeO_2 and ZrO_2, React. Kinet. Catal. Lett. 70 (1) (2000) 97–103.
[33] P. Angevaare, J. Aarden, J. Linn, A. Zuur, V. Ponec, Infrared spectroscopic characterization of the α-Mn_3O_4 surface by adsorption of carbon monoxide, J. Electron Spectrosc. Rel. Phenom. 54 (1990) 795–804.
[34] K.K. Reza, M.A. Ali, M.K. Singh, V.V. Agrawal, A. Biradar, Amperometric enzymatic determination of bisphenol A using an ITO electrode modified with reduced graphene oxide and Mn_3O_4 nanoparticles in a chitosan matrix, Microchim. Acta 6 (184) (2017) 1809–1816.
[35] S.-K. Park, A. Jin, S.-H. Yu, J. Ha, B. Jang, S. Bong, S. Woo, Y.-E. Sung, Y. Piao, In situ hydrothermal synthesis of Mn_3O_4 nanoparticles on nitrogen-doped graphene as high-performance anode materials for lithium ion batteries, Electrochim. Acta 120 (2014) 452–459.
[36] Y. Huang, H. Huang, Q. Gao, C. Gan, Y. Liu, Y. Fang, Electroless synthesis of two-dimensional sandwich-like Pt/Mn_3O_4/reduced-graphene-oxide nanocomposites with enhanced electrochemical performance for methanol oxidation, Electrochim. Acta 149 (2014) 34–41.
[37] Y. Song, R. Zhao, K. Zhang, J. Ding, X. Lv, M. Chen, J. Xie, Facile synthesis of Mn_3O_4/double-walled carbon nanotube nanocomposites and its excellent supercapacitive behavior, Electrochim. Acta 230 (2017) 350–357.
[38] H. Chai, J. Xu, J. Han, Y. Su, Z. Sun, D. Jia, W. Zhou, Facile synthesis of Mn_3O_4-rGO hybrid materials for the high-performance electrocatalytic reduction of oxygen, J. Coll. Interf. Sci. 488 (2017) 251–257.
[39] Y. Wang, H. Guan, C. Dong, X. Xiao, S. Du, Y. Wang, Reduced graphene oxide (RGO)/Mn_3O_4 nanocomposites for dielectric loss properties and electromagnetic interference shielding effectiveness at high frequency, Ceram. Int. 42 (1) (2016) 936–942.
[40] Y. Luo, T. Yang, Z. Li, B. Xiao, M. Zhang, High performance of Mn_3O_4 cubes for supercapacitor applications, Mater. Lett. 178 (2016) 171–174.
[41] L. Malavasi, P. Galinetto, M.C. Mozzati, C.B. Azzoni, G. Flor, Raman spectroscopy of AMn_2O_4 (A = Mn, Mg and Zn) spinels, Phys. Chem. Chem. Phys. 4 (15) (2002) 3876–3880.
[42] G.C. Silva, F.S. Almeida, A.M. Ferreira, V.S.T. Ciminelli, Preparation and application of a magnetic composite (Mn_3O_4/Fe_3O_4) for removal of As (III) from aqueous solutions, Mater. Res. 15 (3) (2012) 403–408.
[43] D.P. Dubal, D.S. Dhawale, R.R. Salunkhe, C.D. Lokhande, Conversion of chemically prepared interlocked cubelike Mn_3O_4 to birnessite MnO_2 using electrochemical cycling, J. Electrochem. Soc. 157 (7) (2010) A812–A817.
[44] Q. Wang, J.-E. Moser, M. Grätzel, Electrochemical impedance spectroscopic analysis of dye-sensitized solar cells, J. Phys. Chem. B 109 (31) (2005) 14945–14953.

[45] W. Zhang, F. Liu, Q. Li, Q. Shou, J. Cheng, L. Zhang, B.J. Nelson, X. Zhang, Transition metal oxide and graphene nanocomposites for high-performance electrochemical capacitors, Phys. Chem. Chem. Phys. 14 (47) (2012) 16331–16337.
[46] M. Govindasamy, S.-M. Chen, V. Mani, M. Akilarasan, S. Kogularasu, B. Subramani, Nanocomposites composed of layered molybdenum disulfide and graphene for highly sensitive amperometric determination of methyl parathion, Microchim. Acta (2016) 1–9.
[47] M. Govindasamy, S.-M. Chen, V. Mani, R. Devasenathipathy, R. Umamaheswari, K.J. Santhanaraj, A. Sathiyan, Molybdenum disulfide nanosheets coated multiwalled carbon nanotubes composite for highly sensitive determination of chloramphenicol in food samples milk, honey and powdered milk, J. Colloid Interface Sci. 485 (2017) 129–136.
[48] M. Govindasamy, V. Mani, S.-M. Chen, B. Subramani, R. Devasenathipathy, S. Tamilarasan, Highly Sensitive Amperometric Sensor for Nitrobenzene Detection Using Functionalized Multiwalled-Carbon Nanotubes Modified Screen Printed Carbon Electrode, Int. J. Electrochem. Sci 11 (2016) 10837–10846.
[49] R. Karthik, M. Govindasamy, S.-M. Chen, V. Mani, R. Umamaheswari, T. Shunmuga Thain Balamurugan, Electrochemical study of nitrobenzene reduction using potentiostatic preparation of nephrolepis leaf like silver microstructure, Int. J. Electrochem. Sci. 11 (2016) 6164–6172.
[50] R. Karthik, M. Govindasamy, S.-M. Chen, V. Mani, B.-S. Lou, R. Devasenathipathy, Y.-S. Hou, A. Elangovan, Green synthesized gold nanoparticles decorated graphene oxide for sensitive determination of chloramphenicol in milk, powdered milk, honey and eye drops, J. Colloid Interface Sci. 475 (2016) 46–56.
[51] S. Das, R. Dubey, S. Roychowdhury, M. Ghosh, B.N. Sinha, K. Kumar Pradhan, T. Bal, V. Muthukrishnan, J.A. Seijas, A. Pujarid, A rapid and sensitive determination of hypoxic radiosensitizer agent nimorazole in rat plasma by LC-MS/MS and its application to a pharmacokinetic study, Biomed. Chromatogr. 29 (10) (2015) 1575–1580.
[52] P. Giriraj, T. Sivakkumar, A rapid-chemometrics assisted RP-HPLC method with PDA detection for the simultaneous estimation of ofloxacin and nimorazole in pharmaceutical formulation, J. Liq. Chromatogr. Relat. Technol. 38 (8) (2015) 904–910.